Physico-chemical changes in biomass chars by thermal oxidation or ambient weathering and their impacts on sorption of a hydrophobic and a cationic compound

Yi Yang[1,2], Pu Duan[3], Klaus Schmidt-Rohr[3], Joseph J. Pignatello[2*]

Submitted to

Environmental Science & Technology

[1] CAS Key Laboratory of Urban Pollutant Conversion, Department of Environmental Science and Engineering, University of Science and Technology of China, Hefei 230026, China

[2] Department of Environmental Sciences, The Connecticut Agricultural Experiment Station, 123 Huntington St., P.O. Box 1106, New Haven, Connecticut 06504-1106, United States

[3] Department of Chemistry, Brandeis University, Waltham MA 02465, USA

*Corresponding author contact information: joseph.pignatello@ct.gov; tel. (1)-203-974-8518

Abstract

This study examined conditions that mimic oxidative processes of biomass chars during formation and weathering in the environment. A maple char prepared at the single heat treatment temperature of 500 °C for 2 h was exposed to different thermal oxidation conditions or accelerated oxidative aging conditions prior to sorption of naphthalene or the dication paraquat. Strong chemical oxidation (SCO) was included for comparison. Thermal oxidation caused micropore reaming, with ambient oxidation and SCO much less so. All oxidative treatments incorporated O, acidity, and cation exchange capacity (CEC). Thermal incorporation of O was a function of headspace O_2 concentration and reached a maximum at 350 °C due to the opposing process of burn-off. The CEC was linearly correlated with O/C, but the positive intercept together with nuclear magnetic resonance data signifies that, compared to O groups derived by anoxic pyrolysis, O acquired through oxidation by thermal or ambient routes contributes more to the CEC. Thermal oxidation increased the naphthalene sorption coefficient, the characteristic energy of sorption, and the uptake rate due to pore reaming. By contrast, ambient oxidation (and SCO) suppressed naphthalene sorption by creating a more hydrophilic surface. Paraquat sorption capacity was predicted by an equation that includes a CEC^2 term due to bidentate interaction with pairs of charges, predominating over monodentate interaction, plus a term for the capacity of naphthalene as a reference representing nonspecific driving forces.

KEYWORDS: organocation sorption; cation exchange; pyrogenic carbons; biochar; black carbon; char oxidation; char weathering; adsorption; solid state ^{13}C NMR

TOC Art

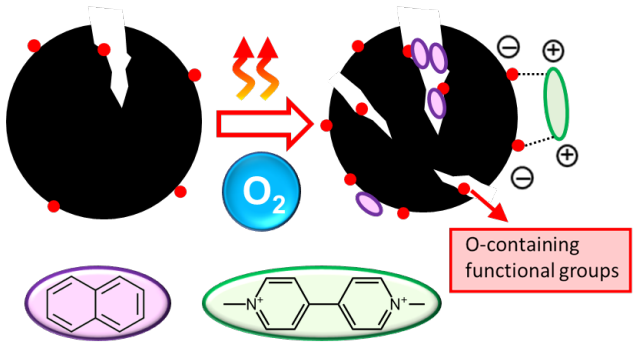

INTRODUCTION

Biomass chars formed as a result of wildfires and intentional burning practices are ubiquitous components of soils and sediments.[1, 2] As part of the black carbon pool, fire-derived chars can impact the carbon cycle[3] and may affect soil microbial community structure[4] and exocellular microbial electron transport processes.[5-7] In many locations chars are sufficiently abundant in soil[8, 9] to play an important role as sorbents affecting the mobility and bioaccessibility of organic contaminants that may be present.[10, 11, 12, 13] Char products synthesized from various biomass wastes ("biochars") have attracted interest as soil amendments to improve soil structure and fertility, suppress greenhouse gas emissions,[14, 15] and reduce the availability of soil pollutants.[15] Many of the desired functions of biochars depend critically on their sorptive properties towards small molecules and ions.

The sorptive properties of chars vary with source material and pyrolysis conditions, including temperature, time and rate of heating, and headspace gas composition. These variables can influence specific surface area, pore size distribution, aromatic C content, degree of aromatic condensation, and surface functional group composition.[11, 16, 17] Oxygen may be incorporated into chars during pyrolysis when O_2 is present in the surrounding gas, as well as during weathering in the environment. Biomass in open fires is exposed to varying oxygen concentration as it burns. Biochars are ordinarily made in the absence or near absence of air. Air is often difficult to rigorously exclude in large scale reactors, and is sometimes intentionally introduced to initiate sustained pyrolysis or favor production of bio-oils. Chars deposited in soils or aquatic sediments are susceptible to air oxidation and enzyme-induced oxidation over time. The introduction of O during pyrolysis or weathering can greatly affect the physico-chemical and sorptive properties of chars, but such effects have hardly been investigated in any systematic way.

Tomkow et al.[18] report that re-heating brown coal chars in O_2 increased or decreased porosity and surface area depending on temperature and degree of burn-off. From the CO_2 evolution profiles on re-heating, the O content of nut shell and coconut shell charcoals reached steady state at a given O_2 concentration and temperature due to opposing processes of incorporation and burn-off.[19] Xiao and Pignatello[19, 20] found that brief reheating of

anoxically-produced wood chars in air at 400 °C enlarges both micropores and mesopores and introduces acidic groups, leading to significant increases in sorption of various organic compounds from water.

Other studies have reported on aging of chars in ambient or warm air or under 'accelerated' weathering conditions. Immediately after their preparation, chars chemisorb considerable amounts of oxygen and water from ambient air over weeks due to reactive sites generated during pyrolysis.[21, 22] Artificial accelerated aging has had mixed effects on specific surface area (SSA), some studies reporting a decrease (eucalyptus treated with H_2O_2[23]), while others little or no change (corn stover biochars and an activated carbon in moist air at 60°C or 110°C for 2 months[24]). Environmental aging of oak, pine, and grass chars for 15 months reduced N_2-B.E.T. SSA, but CO_2-SSA varied greatly.[25] Accelerated chemical aging can also increase O/C atomic ratio and cation exchange capacity (CEC).[24,26] Little research has been reported on the inherent effects of aging on sorption, however. Hale et al.[24] found that accelerated chemical aging of corn stover biochars slightly reduced the Freundlich sorption coefficient of pyrene. Although aging of chars in soil mixtures often decreases their ability to sorb organic compounds,[10, 27, 28] an interpretation of this outcome is complicated by the transfer to char surfaces of soil organic matter, which can compete for sorption sites and clog pores.[29] The overall objectives of this project are to determine the underlying structural and chemical alterations of char caused by thermal and ambient oxidation regimes, and to determine effects of these alterations on interactions with pollutants. To date, little clear and quantitative understanding about how surface O incorporation and pore structural modification due to oxidation and weathering interplay to affect sorption. Moreover, little research has been done on sorption of organocations, and none on dications, in the context of char formation and weathering conditions.

This study examined and compared the effects of thermal oxidation and simulated weathering of chars on sorption of different model compounds. The base char is from a hardwood treated at 500 °C, which is intermediate in the normal temperature range experienced in fires and used to make biochars. Sorption to this series of chars is assumed to occur predominantly by adsorption and pore filling mechanisms. One model compound is naphthalene, representative of compounds associating with carbonaceous materials by

non-specific driving forces (van der Waals, hydrophobic effect), where surface area and pore size distribution as well as surface hydrophilicity are important. The other is the aquatic herbicide paraquat (*N*,*N*'-dimethyl-4,4'-bipyridinium, also known as methyl viologen), which is a permanently charged dication whose sorption depends additionally on electrostatic forces (Coulombic and charge-dipole). These two compounds were used as contrasting probes to gage the consequences of changes in the physical-chemical properties of chars exposed to thermal or ambient oxidation conditions. The results show profound effects of thermal and ambient oxidation on the structure, chemical properties, and sorptivity of chars. They reveal sharp contrasts between chars exposed to thermal compared to ambient conditions, and between neutral compounds versus organocations. The results provide new insight into mechanism and augment previous conclusions[20, 30].

Experimental Section

Sorbents

The base char (hereafter, "original char") was made from ~1-mm thick maple wood shavings placed in the tubular quartz chamber of a temperature- and atmosphere-controlled three-zone tube furnace (LindbergBlue Model STF55666C) with a continuous flow of desired gas at 1.5 L/min (Figure S1, Supplementary Information section). The sample was heated in N_2 flow to 100 ^oC (7 ^oC/min) and held at that temperature for 1 h, then to 500 ^oC (25 ^oC/min) and held for 2 h (Figure S1). The product was allowed to cool to room temperature in the furnace with continued N_2 flow. Several batches were combined and gently pulverized to pass a 0.15 mm sieve.

Thermal oxidation. To simulate thermal air oxidation during charring we employed two different hot O_2 exposure conditions: (i) The feedstock was pyrolyzed in the same way as the original char at 500 ^oC, except in the presence of O_2 at 1% or 2% O_2 in N_2 (Figure S1). This treatment is labelled Concurrent-with-Pyrolysis Air Oxidation (CPAO). (ii) The original char was re-heated in the presence of O_2 at different concentrations (1%, 5%, or 21% O_2 in N_2) and temperatures (250, 300, 350, 400, or 450°C) (Figure S1). This treatment is labelled Post-Pyrolysis Air Oxidation (PPAO).[19, 20]

150 *Ambient weathering.* We employed two different accelerated exposure conditions,
151 starting with the original char. These treatments are labelled Accelerated Ambient Air
152 Oxidation (AAAO). Soil and microorganisms were omitted to eliminate secondary effects
153 on sorption from introduced soil and microbial organic matter.

154 (i) Samples labeled AAAO-H_2O_2 were prepared by treating original char (4 g)
155 repeatedly with 50-mL portions of hydrogen peroxide (refreshed daily) with tumbling over
156 ten days at room temperature. The H_2O_2 was completely consumed after each 24-h period.
157 This treatment was performed to simulate oxidation by reactive oxygen species (mainly
158 hydroxyl radical) generated abiotically or through enzymatic activity in soil.

159 (ii) Samples labelled AAAO-O_2 were prepared by exposing original char (10 g)
160 contained in a 9-cm diameter petri dish and placed in a desiccator at a slight positive
161 pressure of O_2 at 100% relative humidity for 180 days at 60°C (see Figure S2). The
162 conditions were meant to simulate accelerated chemical oxidation by air.

163 *Strong chemical oxidation.* For reference, we also examined original char treated by
164 strong chemical oxidation (SCO) using warm nitric acid (SCO-NA) or ammonium
165 persulfate (SCO-APS). Nitric acid is widely used to increase the acidity of carbonaceous
166 surfaces (detailed in Text S1).[31-33]

167 **Sorbent characterization**

168 Samples were characterized for the following: electrokinetic (zeta) potential (Malvern
169 Zetasizer Nano ZS90); CHNO elemental composition (Costech ECS 4010); acidic content
170 (carboxylic, lactonic, phenolic) by Boehm's titration;[34] cation exchange capacity (CEC) at
171 pH 7.4 (the same pH as sorption) by the ammonium acetate method[35]; and micropore
172 (≤1.47 nm) surface area and pore size distribution by CO_2 porosimetry (Autosorb IQ,
173 Anton Paar) at 273 K after outgassing at 200°C. [20] Solid-state ^{13}C NMR spectra were
174 recorded on a Bruker Neo WB400 spectrometer at a ^{13}C frequency of 100 MHz, using a
175 Bruker 4-mm double-resonance magic-angle spinning (MAS) probe head at a rotation
176 frequency of 14 kHz. The NMR techniques used are described in the SI.

177

178 **Sorption**

179 Sorption of naphthalene or paraquat (Sigma-Aldrich) was conducted by the batch method
180 in 60-mL glass or 15-mL polypropylene vials, respectively. Char (5-40 mg) was pre-wetted
181 for 48 h with water adjusted to pH 7.4 ±0.2 with NaOH or HCl (naphthalene) or buffered
182 at pH 7.4 with 50 mM phosphate (paraquat). Preliminary tests (Figure S3) showed
183 polypropylene vials were essential for paraquat, a bio-inhibitor like azide was unnecessary,
184 and there was no interference by the buffer. Paraquat appeared stable under the conditions
185 (Text S1). After test compound addition, vials were mixed end-over-end (20 rpm) in an
186 incubator at 20 °C for 7 d, by which time tests showed uptake had leveled off. A portion
187 of the supernatant phase was filtered (0.45 μm PTFE) and the solute concentration
188 determined by HPLC, as described in Text S1.

189 Sorption curves were fit to the Freundlich, Langmuir, or Dubinin-Ashtakhov models
190 for various purposes.[36] The Freundlich is given by:

191 $$q = K_F C_w^{\ n} \qquad (1)$$

192 where q (mass-normalized or surface area-normalized units, mg/kg or mg/m^2) and C_w
193 (mg/L) are the equilibrium sorbed and solution-phase concentrations, respectively; K_F
194 (mg^{1-n}L^{n}kg^{-1} or mg^{1-n}L^{n}m^{-2}) is the affinity coefficient; and n is the linearity parameter.
195 Comparison among different chars is possible at unity solute concentration (1 mg/L), where
196 K_F is independent of n.

197 The Langmuir model is given by:

198 $$q = \frac{Q^0_L K_L C_w}{1 + K_L C_w} \qquad (2)$$

199 where Q^0_L is the maximum adsorption capacity and K_L is an equilibrium constant.

200 The Dubinin-Ashtakhov[37, 38] (D-A) model is given by:

201 $$\log q = \log Q^0_{DA} - \left(\varepsilon / E_{DA}\right)^b; \qquad \varepsilon = -RT \ln\left[C_w / C_w^{sat}(L)\right] \qquad (3)$$

where Q^0_{DA} is adsorption capacity; ε (kJ/mol) is the effective adsorption potential; $C_w^{sat}(L)$ is the sub-cooled liquid water solubility at 298 K (106.6 mg/L for naphthalene[39] which melts at 80 °C); R is the gas constant; T (in K) is absolute temperature; b is a heterogeneity parameter;[40]; and E_{DA} is the characteristic adsorption energy (kJ/mol), which includes all forces of direct interaction between the molecule and the surface.[41, 42] E_{DA} is independent of units of normalization, whether mass or SSA. (Note that the D-A model is not suitable for paraquat since $C_w^{sat}(L)$ is undefined.) Fits to all models were obtained by weighted non-linear regression using Origin.

When only single-point sorption data were compared, as in the pH-dependence experiments, the (concentration-dependent) distribution ratio K_d was calculated by:

$$K_d = \frac{q}{C_w} \quad (4)$$

Results and Discussion

Effects on Physico-chemical Properties

Surface area and porosity. The emphasis of this study is on micropores, which contain the majority of surface area in chars.[17, 43] Generally, most (85%–91%) of the CO_2-specific surface area (CO_2-SSA) lay in ultramicropores (0.35–0.7 nm) with the remainder in supermicropores (0.7–1.47 nm) (Figure S4). For PPAO samples, CO_2-SSA generally increases with headspace O_2 content at a given PPAO temperature, and the rate of increase with pore width trends positively with PPAO temperature. Likewise, microporosity increased with O_2 content and temperature, especially in the supermicropore region (Figures 1a and Figure S5). The effect of PPAO depends also on the thermal history of the char: chars prepared at 500 °C (this study) or 400 °C[20] and then treated under identical PPAO conditions experience a 32% or 100% increase, respectively, in CO_2-SSA.

Chars made under CPAO conditions showed trends in the same direction as PPAO-treated chars: maple wood exposed to 1% or 2% O_2 during pyrolysis had, respectively, 23% or 25% greater CO_2-SSA (Figure S4) and 31% or 34% greater microporosity (Figure S5) than the original char created in the absence of O_2. Hot oxygen attacks pore walls and

entrained substances in the pores, resulting in their volatilization as CO_2, CO, H_2O, and small organic molecules.[20] The increase in CO_2-SSA during PPAO and CPAO is attributable to the combined processes of pore wall etching and oxidative removal of entrained substances, which we refer to as reaming.[20]

Ambient oxidation also increased surface area (Figure S4) and microporosity (Figure S5), but less so than thermal oxidation. Samples AAAO-O_2 and AAAO-H_2O_2 experienced increases in CO_2-SSA of 15% and 11%, respectively, relative to the original char. These small changes are consistent with the small and variable changes reported in the literature.[23-25] The increases were proportionately greater in supermicropores (21%) than ultramicropores (18%). By contrast, strong chemical oxidation (SCO-NA or SCO-APS) had slightly negative effect: the CO_2-SSA decreased by 4% and 5%, and the microporosity by 7% and 6%, respectively.

Acidity, surface charge, and cation exchange capacity. All oxidative treatments incorporated O into the char, as evidenced by O/C atomic ratio (Table S1) and acidity (Table S1, Figure S6). Acidity universally followed the order, carboxylic (pK_a = 5.15–6.11) > phenolic (pK_a = 10.5–10.8) > lactonic (pK_a = 7.36–8.26) (Figure S6). Acidity after thermal oxidation, a) increased with headspace O_2 concentration at each PPAO temperature; b) reached a maximum at the intermediate PPAO temperature of 350 °C at each headspace O_2; and c) increased with headspace O_2 during CPAO. Both AAAO conditions, especially AAAO-H_2O_2, were considerably less effective than thermal oxidation at introducing acidity. Both SCO treatments, especially SCO-NA, boosted O/C.

All oxidative treatments introduced negative charges as indicated by zeta potential vs pH curves between 3 and 7 (Figure S7) and CEC measurements (Figure 1b). At a given pH, zeta became more negative with increasing headspace O_2 for both PPAO and CPAO. Along the PPAO temperature series, zeta reached minimum at 350 °C. AAAO-O_2 and AAAO-H_2O_2 also gave negative zeta, especially the former. SCO treatments gave the most negative zeta values of all.

The CEC (Figure 1b) after thermal treatments generally increased with headspace O_2 concentration and reached a maximum at 350 °C along the PPAO temperature series. PPAO at the highest O_2 level (21%) and SCO-NA were the most effective of all treatments

at introducing CEC. The CEC correlates strongly with titration acidity at pH 7.4 (namely, the sum of carboxylic and lactonic groups[44]), passing through the origin (Figure S8). The CEC also correlates strongly with O/C atomic ratio (Figure 1c), but interestingly intersects the O/C axis at a positive value (0.073). This suggests that little of the O present in woody biomass chars formed under anoxic conditions is converted into CEC, and that most CEC of chars and biochars originates from thermal oxidation when air is present or from oxidation during environmental weathering. This is confirmed by NMR in the next section.

Functional group composition by NMR spectrometry. ^{13}C NMR spectrometry can be used to quantify aromatic C, alkyl C and certain O-functional groups (Ar-C-O, Ar-COO, and Ar-C=O). The PPAO-21%O_2 temperature series was selected for ^{13}C NMR analysis (spectra in Figures S9-S10). The dominant signals appear between 100 and 210 ppm, corresponding to Ar-C=C (95-145), Ar-C-O (145-160), Ar-COO (165-175), and Ar-C=O (>175), where Ar stands for aromatic. Their relative concentrations are plotted in Figure S11. All the O-containing functional groups show a clear maximum at 350°C. The non-oxygenated sp^3-C signal (<60 ppm) decreases with PPAO temperature due to oxidation of alkyl groups. At higher temperature, some of the O groups are thermally removed and replaced by H, resulting in an increase in alkyl C. These results demonstrate conversion of alkyl C to CO or COO, and then the depletion of CO or COO at higher temperature.

The O-functional group composition and O/C ratio estimated by NMR and elemental analysis for the PPAO-21%O_2 series appears in Figure 1d. Spectra of ^{13}C-enriched glucose char samples were used as an aid to distinguish the contributions to Ar-C-O of phenolic and aromatic ether,[45] which cannot be resolved by natural abundance ^{13}C-NMR (see Text S2). Aromatic ether is mostly furan groups. Agreement between the NMR- and elemental analysis-estimated values of O/C is good (Figure 1d). The original char contains a lot of furans and some C=O groups, but hardly any COOH groups. This explains the intersection of the CEC curve at a positive value of the O/C axis in Figure 1c. PPAO at or below 350 °C generates COOH, COOC, C=O, and C-OH and slightly reduces furan content, accounting for the rise in O/C and CEC. Above 350 °C, COOH, COOC, and phenolic content are lost by burn-off, which is responsible for the decline in O/C and CEC.

In summary to this point, thermal oxidation causes pore size expansion and introduces acidic groups. Along the PPAO thermo-series, changes in acidity, elemental O, zeta potential, CEC, and various O functional group NMR intensities peak at 350 °C. Such results are consistent with dual processes of O-incorporation by the hot gas, opposed by O-removal via thermal decarboxylation and decarbonylation reactions.[33] AAAO treatments lead to O-incorporation, but only slight pore modification.

Effects on Naphthalene Sorption

Sorption isotherms appear in Figure S12-S16 and model parameters in Tables S2-S4. Thermal and ambient oxidation have very different effects on naphthalene sorption (Figure 2a). For PPAO-treated samples, CO_2-SSA-normalized $K_{F,nap}$ at unity concentration trends upward with both headspace O_2 concentration and PPAO temperature, reaching a maximum for the PPAO-450-21%O_2 sample of 20.7 times the $K_{F,nap}$ of its control, PPAO-450-N_2. (Note that $K_{F,nap}$ for the controls at each PPAO temperature differed little from each other and from the original char and showed no trend.) For CPAO samples, $K_{F,nap}$ exceeds that of the original char by a factor of 12 for CPAO-2%O_2 and 10.4 for CPAO-1%O_2 char. The corresponding mass-normalized values (Figure S17) show the same trends, which indicates that surface area is not the only underlying cause of naphthalene sorption enhancement by thermal oxidation.

In contrast to thermal oxidation, ambient oxidation *suppresses* naphthalene sorption relative to the original char (Figure 2a). $K_{F,nap}$ was decreased by a factor of ~11 for AAAO-H_2O_2 and ~4 for AAAO-O_2 compared to the original char. Strong chemical oxidation (SCO-NA and SCO-APS) also reduced $K_{F,nap}$ of naphthalene, by ~4-fold in each case.

We pose a unified mechanism to account for the effects of thermal and ambient oxidation on naphthalene sorption, which is discussed in this and the next two paragraphs. Thermal oxidation acts to ream pores by etching pore walls and volatilizing entrained organic matter within the pores.[20, 30] As a consequence, it causes a general increase in surface area and porosity. Reaming creates additional sorption space and acts to remove obstructions from pore throats, thereby improving access to sorption sites. To test the pore-obstruction hypothesis, rates of naphthalene uptake were measured for the PPAO-450 series (Figure 2b). Mass taken up was normalized by mass finally taken up (m_t/m_{max}) to

allow direct comparison among chars having different equilibrium affinity for naphthalene.[46] Rate of uptake below m_t/m_{max} of 0.9 follows the order in headspace O_2 content: $0\%O_2 < 1\%O_2 < 5\%O_2 \approx 21\%O_2$, which is the same as the order of change in cumulative pore volume of the micropores relative to the control (Figures 1a and S5). This result implies that pore reaming enhances pore diffusion of naphthalene and/or alleviates steric hindrance at previously obstructed pore openings.

By contrast with thermal oxidation, ambient oxidation has a weaker effect on surface area and pore volume, which suggests it does not ream pores or remove obstructions as effectively. Nevertheless, ambient oxidation substantially increases acidity (Figure S6), surface charge (Figure S7), O/C ratio (Table S1), and CEC (Figure 1b) relative to the original char, and thus leads to materials that retain the chemical effects of O introduction. SCO can be regarded as the extreme case of ambient oxidative weathering in this regard. We propose that introduction of O by AAAO and SCO suppresses naphthalene sorption by attracting water molecules, which cluster around polar groups, reducing the surface area/pore volume available for sorption.[47-50] This "crowding-out" hypothesis is backed by molecular simulations of methane and water adsorption on hydrophobic surfaces populated by different densities of polar sites.[51, 52] The pH dependence of naphthalene sorption supports it: Figure 2c shows that $K_{d,nap}$ for the PPAO-400 series decreases as pH increases from 1.5 to 11.5, especially at the extreme ends of this range. The change is small—less than 3-fold—but greater at the higher than at the lower headspace O_2 concentration. A reasonable explanation consistent with the crowding-out hypothesis is that ionization favors hydration.

Figure 2d (red points, right scale) shows that the Dubinin-Ashtakhov characteristic sorption energy (E_{DA}) of naphthalene increases with thermal oxidation for the PPAO and CPAO samples relative to the respective control. By contrast, E_{DA} values for AAAO and SCO samples are unchanged from the control. A recent experimental and theoretical study identified two properties of char that potentially lead to an increase in E_{DA}: *i*) the degree of aromatic condensation (related to aromatic ring cluster size), which affects dispersion forces with sorbates; and ii) an increase in microporosity in (slit-shaped) pores bounded by

aromatic sheets, which favors monolayer or bilayer sorption in pores over sorption to an open surface.

Degree of aromatic condensation is not a viable explanation for the increase in E_{DA} with thermal oxidation because the NMR-determined fraction of bridgehead aromatic carbon (χ_b), which is a measure of ring cluster size,[32] is not affected by PPAO treatment (Table S5). An increase in microporosity, however, is a plausible explanation. For phenol, the computed molar binding energy between parallel-planar polyaromatic sheets is strengthened for inter-sheet widths above ~0.59 nm: widths between 0.59-1.0 nm favor monolayer sorption in the pore over monolayer sorption on an open sheet; whereas widths above ~1 nm (an upper width was not defined) favor bilayer sorption over monolayer sorption in the pore. Similar behavior should be expected for naphthalene, although the widths may be slightly different. Figure 1a and S5 show that cumulative microporosity in 0.59-1.47 nm pores increases more steeply relative to the control in thermal oxidized compared to ambient oxidized samples, with the thermal oxidized samples showing an upward trend as headspace O_2 and PPAO temperature rise. Figure 2d displays stacked bars showing the difference in cumulative micropore volume within a desired interval (ΔV) relative to the control, $\Delta\Delta V = \Delta V$(sample) - ΔV(control), in each of the two intervals, 0.59-1.0 nm and 1.0-1.47 nm. The overall ($\Delta\Delta V_{0.59\text{-}1.47}$) and each sub-interval ($\Delta\Delta V_{0.59\text{-}1.00}$ and $\Delta\Delta V_{1.00\text{-}1.47}$) trends with E_{DA}, although the correlation is not strong in any case. The trend suggests that the increase in microporosity due to pore reaming by thermal oxidation increases the energy of sorption, while just populating the surfaces with O groups does not.

Effects on Paraquat Sorption

Figure 3a shows that, like naphthalene, CO_2-SSA normalized $K_{F,para}$, a) increases after thermal oxidation, b) trends positively with headspace O_2 concentration at a given PPAO temperature, and c) trends positively with PPAO temperature at a given headspace O_2 concentration. Also, like naphthalene, the CO_2-SSA-normalized $K_{F,para}$ is much more strongly affected by thermal than by ambient oxidation. Those conclusions are unchanged by normalizing $K_{F,para}$ to char mass units (Figure S18).

In contrast to naphthalene, paraquat is ionic and expected to be more sensitive to surface charge density. Figure 3a and S18 show that $K_{F,para}$ maximizes at PPAO of 350 °C, where O/C and CEC maximize (Figures 1b and 1c) and zeta potential minimizes (Figure S7); thus confirms the importance of charge pairing for paraquat. The maximum observed value of $K_{F,para}$ is ~700 times greater than $K_{F,para}$ of the control. Ambient oxidation also caused a slight increase in $K_{F,para}$ (AAAO-O_2 > AAAO-H_2O_2) in step with an increase in CEC and a decrease in zeta potential, but the changes are far less than caused by thermal oxidation. Strong chemical oxidation increased $K_{F,para}$ by a factor of 90 for SCO-NA and 16.6 for SCO-APS, consistent with increases in CEC and decreases in zeta. Lastly, Figure 3b shows that $K_{d,para}$ for the PPAO-400 series is highly sensitive to pH, increasing by up to 1000 fold over the test range (pH 1.5 to 10-12)—far greater than the changes observed for naphthalene. The steepness of the $K_{d,para}$ *vs* pH curve follows the order in CEC at pH 7.4, 1% O_2 < 5% O_2 < 21% O_2 chars (Figure 1b). These results demonstrate that the increase in $K_{d,para}$ is due to the buildup of surface charge as acidic groups become deprotonated.

Nevertheless, sorption maximum capacity ($Q^0_{L,para}$) correlates quite poorly with CEC and gives an unrealistic (negative) intercept: $Q^0_{L,para} = 0.81 \cdot CEC - 11.60$ ($r^2 = 0.51$) (Figure S19). This can be rationalized by considering multiple modes of interaction. We postulate that paraquat sorbs simultaneously as: the neutral ion triplet PX_2 composed of P^{2+} and its two (monovalent) counterions X^- (eq 5); the monocation ion pair PX^+ (eq 6); and the dication P^{2+} (eq 7).

$$P^{2+} + 2X^- + s \rightleftharpoons PX_2{:}s \quad (5)$$

$$P^{2+} + X^- + M{:}s \rightleftharpoons PX{:}s + M^+ \quad (6)$$

$$P^{2+} + 2M{:}s \rightleftharpoons P{:}ss + 2M^+ \quad (7)$$

where s represents a site and M^+ is the native exchangeable cation (Na^+ here, as sodium phosphate was the background electrolyte).

Sorption of PX_2 (eq 5) may be regarded as driven primarily by non-specific (NS) forces such as van der Waals and the hydrophobic effect, subject to steric constraints that govern efficient packing in pores. Sorption of PX_2 in this way is congruent with the tendency of organocation salts to sorb maximally to environmental sorbents in excess of

405 the CEC, which has been explained in terms of a "hydrophobic" component of the total
406 sorption free energy due to the ion's vicinity to the surface.[53] In the thermodynamic
407 formalism of the Langmuir model it is to be regarded as a competition between solute and
408 water molecules for NS-type sites, with maximum capacity $Q_{L,para}^{NS}$.

409 The PX^+ and P^{2+} species are regarded to sorb by ion exchange. According to diffuse
410 double layer theory, ions considered sorbed occupy a thin water layer near the surface
411 (vicinal water). While this concept may reflect reality for open, unhindered mineral
412 surfaces, ions confined in the nanopores of chars, where van der Waals/hydrophobic effects
413 are experienced in addition to Coulombic forces, may more closely associate in space with
414 surface charges. Thus, PX^+ and P^{2+} would interact, respectively, *via* monodentate ion
415 pairing (MIP; eq 6)) and bidentate ion pairing (BIP; eq 7). The BIP interaction is depicted
416 here,

417 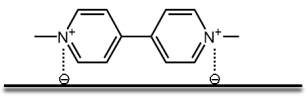

418 BIP is expected to be energetically more favorable than MIP, but requires that surface
419 charges be appropriately spaced. Theoretical studies have revealed preferential BIP of the
420 analogous dication, 4,4'-bipyridinium, to charges in the nanopores of H-ZSM-5 zeolite.[55]

421 Langmuir expressions for sorption of PX^+ and P^{2+} may be derived based on
422 thermodynamic competition between solute and M^+ for coulombic sites (Text S3).
423 Assuming the site density is equal to the CEC, it can be shown (Text S3) that the respective
424 Langmuir maximum capacities are,

425 $$Q_{L,para}^{MIP} = \frac{CEC}{[M^+]} \quad (8)$$

426 $$Q_{L,para}^{BIP} = \frac{f \cdot CEC}{[M^+]^2} \quad (9)$$

427 where $[M^+]$ is the aqueous native metal ion concentration and f is the fraction of CEC sites
428 spaced suitably to undergo BIP with paraquat.

429 The total Langmuir maximum capacity of paraquat can then be written,

$$Q^{0}_{L,para} = Q^{NS}_{L,para} + Q^{MIP}_{L,para} + Q^{BIP}_{L,para} \quad (10)$$

Since paraquat has similar electronic and steric properties as naphthalene except for charge, we may consider naphthalene as a reference for NS forces governing paraquat sorption and write,

$$Q^{NS}_{L,para} = a \cdot Q^{0}_{L,nap} \quad (11)$$

where a is a proportionality factor.

The fraction f in eq 11 is not a constant but is proportional to the probability P that paired charges are spaced apart by $d + x$ or $d - y$ where d is the interatomic distance between charge centers and x and y are tolerance distances. Thus, P is a function of charge density (CEC), d, x, and y. If we assume randomly distributed point charges, P can be estimated by the Poisson distribution, which in turn can be expressed as a power law with respect to CEC for various x and y (Text S3):

$$f \propto P \cong const \cdot \mathrm{CEC}^{n} \quad (12)$$

where *const* is a constant and n is an exponent (Text S3, Figure S20). Given the experimental range of SSA-normalized CEC (0.0214 to 0.42 nm^{-2}; Table S1) and the computed d between N atoms in the longitudinally-rigid paraquat of 0.711 nm,[54] and choosing reasonable values for the tolerance (x = 0.01-0.6 nm; y = 0.01-0.4 nm), n is found to vary from 0.7602-0.9951. In other words, f is close to being linearly dependent on CEC in this hypothetical system. A different range in n might be obtained if the surface charge distribution were not random, or if the charge densities were higher or lower than those in this range.

Substituting eqs 8,9 and 11 into eq 10, taking n = 1, and assuming constant pH and $[M^{+}]$ gives an expression of the form:

$$Q^{0}_{L,para} = a \cdot Q^{0}_{L,nap} + b \cdot \mathrm{CEC} + c \cdot \mathrm{CEC}^{2} \quad (13)$$

where a, b, and c are regression coefficients.

Accordingly, we performed multiple linear regression, equating $Q^{0}_{L,para}$ with terms for CEC, CEC^2, and $Q^{0}_{L,nap}$ (all in units of 10^{-3}·mol/kg) (Table S6). Considering the p-value of

terms (<0.05 indicating a significant predictor) and the R-square in regression analysis, the best correlation obtained for all chars subjected to PPAO, CPAO, AAAO-O_2, or AAAO-H_2O_2 treatment is:

$$Q^0_{L,para} = 0.12\ Q^0_{L,nap} + 0.0023\ CEC^2 \quad R^2 = 0.875 \qquad (14)$$

Regressions combining CEC with just CEC^2, or CEC with both CEC^2 and $Q^0_{L,nap}$ terms, gave poorer fits, and the latter combination gave an unrealistic negative coefficient for CEC. Figure 3c plots the predicted (based on eq 14) vs experimental values of $Q^0_{L,para}$. Including SCO-NA and SCO-APS data invariably worsened the correlation (Figure S21); nevertheless, the best correlation (eq S7; $R^2 = 0.757$) is analogous to eq 14 with slightly different coefficients. Regressions based on eq 14 but increasing the exponent of CEC *n* to 1.75 or 1.9 gave slightly different value of *a* (0.11) but did not substantially change the R^2 value (0.865 and 0.872, respectively). The insignificance of the *b*·CEC term in eq 13 implies that bidentate association is stronger than monodentate association.

The results clearly show that paraquat sorption capacity is predominantly a function of dication-charge pair forces in addition to non-specific driving forces proportional to those of the reference, naphthalene. The CEC plays a growing role in paraquat sorption as CEC increases. For example, dication-charge pair interaction contributes only 5% of $Q^0_{L,para}$ for the PPAO-450-21%O_2 sample (CEC = 69.2 $mmol_c/kg$), but 82% of $Q^0_{L,para}$ for the PPAO-350-21%O_2 sample (CEC = 407 $mmol_c/kg$). This is apparently the first report showing experimentally that organo dications interact predominantly in a bidentate fashion with pairs of charges on a carbonaceous surface and that their sorption obeys a square dependence on CEC. Finally, the coefficient of $Q^0_{L,nap}$ indicates that driving forces controlling naphthalene sorption collectively are only ~12% as effective for paraquat sorption, certainly due to the great difference in polarity, which favors partitioning of paraquat into water.

A detailed analysis has revealed how thermal and ambient oxidation alter surface chemistry and rebuild pore structure in ways that impact sorption of hydrophobic and charged compounds. Thermal oxidation causes pore enlargement, while ambient oxidation has little effect on pore physical properties. Pore reaming increases available sorption space, enhances the sorption strength, and removes steric barriers to equilibrium. While all

oxidative treatments incorporate O into chars, ambient oxidation is much less effective at introducing cation exchange capacity. Incorporation of O and CEC during thermal oxidation reaches maximum values at 350°C due to opposing generation and burn-off processes. The base char has little O in CEC functional groups, whereas O acquired through thermal or ambient oxidation is efficiently incorporated into CEC. This finding will prove useful for designing biochars with enhanced CEC. Populating surfaces with O groups also has an inhibiting effect on sorption. Inhibition is due to competition by water molecules. In the case of thermal oxidation, inhibition due to water competition opposes enhancement due to pore reaming. Paraquat responds strongly to CEC. Paraquat sorption capacity is proportional to CEC^2 due to its preferred bidentate association with dual charged sites. Nonspecific driving forces also play a role. The findings of this study not only have implications for the mobility of organic compounds in the environment, but also for tailoring adsorbents in remediation or stabilization of contaminated soils. PPAO is a simple and effective way to modify engineered biochars for greater sorption affinity. CPAO can be a potential production process for biochar.

ACKNOWLEDGEMENTS

This project was supported by grants from the National Science Foundation of the United States (CHE-1709532 and CHE-1709614). The solid-state NMR spectrometer used in this work was funded by the NSF MRI program (Award No. 1726346).

SUPPLEMENTARY INFORMATION

Additional details on materials and methods, pore volume and pore size distribution, functional oxygen groups, zeta potential, NMR spectra, naphthalene and paraquat sorption isotherm, sorption fitting parameters using Freundlich, Dubinin-Ashtakhov and Langmuir model appear in the Supporting Information which is available free of charge on the ACS Publications website at DOI:***.

REFERENCES

1. Skjemstad, J. O.; Reicosky, D. C.; Wilts, A. R.; McGowan, J. A., Charcoal Carbon in U.S. Agricultural Soils. *Soil Sci. Soc. Am. J.* **2002,** *66*, 1249-1255.
2. Schmidt, M. W.; Noack, A. G., Black carbon in soils and sediments: analysis, distribution, implications, and current challenges. *Global Biogeochem. Cycles* **2000,** *14*, 777-793.
3. Bird, M. I.; Wynn, J. G.; Saiz, G.; Wurster, C. M.; McBeath, A., The Pyrogenic Carbon Cycle. *Annual Review of Earth and Planetary Sciences.* **2015,** *43*, 13-54.
4. Theis, J.; Rillig, M. C.; Graber, E. R., Biochar effects on the abundance, activity and diversity of the soil biota. In *Biochar for Environmental Management. Science, Technology and Implementation*, Second ed.; Lehmann, J.; Joseph, S., Eds. Routledge: New York, NY, 2015; pp 327-390.
5. Cayuela, M. L.; Sánchez-Monedero, M. A.; Roig, A.; Hanley, K.; Enders, A.; Lehmann, J., Biochar and denitrification in soils: when, how much and why does biochar reduce N 2 O emissions? *Sci. Rep.* **2013,** *3*, 1-7.
6. Kappler, A.; Wuestner, M. L.; Ruecker, A.; Harter, J.; Halama, M.; Behrens, S., Biochar as an Electron Shuttle between Bacteria and Fe(III) Minerals. *Environmental Science & Technology Letters* **2014,** *1*, 339-344.
7. Klüpfel, L.; Keiluweit, M.; Kleber, M.; Sander, M., Redox Properties of Plant Biomass-Derived Black Carbon (Biochar). *Environ. Sci. Technol.* **2014,** *48*, 5601-5611.
8. Lehmann, J.; Skjemstad, J.; Sohi, S.; Carter, J.; Barson, M.; Falloon, P.; Coleman, K.; Woodbury, P.; Krull, E., Australian climate–carbon cycle feedback reduced by soil black carbon. *Nature Geoscience* **2008,** *1*, 832.
9. Mao, J. D.; Johnson, R. L.; Lehmann, J.; Olk, D. C.; Neves, E. G.; Thompson, M. L.; Schmidt-Rohr, K., Abundant and Stable Char Residues in Soils: Implications for Soil Fertility and Carbon Sequestration. *Environ. Sci. Technol.* **2012,** *46*, 9571-9576.
10. Kwon, S.; Pignatello, J. J., Effect of Natural Organic Substances on the Surface and Adsorptive Properties of Environmental Black Carbon (Char): Pseudo Pore Blockage by Model Lipid Components and Its Implications for N2-Probed Surface Properties of Natural Sorbents. *Environ. Sci. Technol.* **2005,** *39*, 7932-7939.
11. Zhu, D.; Kwon, S.; Pignatello, J. J., Adsorption of Single-Ring Organic Compounds to Wood Charcoals Prepared under Different Thermochemical Conditions. *Environ. Sci. Technol.* **2005,** *39*, 3990-3998.
12. Pignatello, J. J., Interactions of Anthropogenic Organic Chemicals with Natural Organic Matter and Black Carbon in Environmental Particles. In *Biophysico-Chemical Processes of Anthropogenic Organic Compounds in Environmental Systems*, Xing, B.; Senesi, N.; Huang, P. M., Eds. J. Wiley & Sons: Hoboken, New Jersey, U.S.A., 2011; pp 3-50.
13. Pignatello, J. J., Adsorption of Organic Compounds by Black Carbon from Aqueuous Solution. In *Molecular Environmental Soil Science*, Xu, J.-M.; Sparks , D. L., Eds. Springer: 2013; pp 359-385.
14. Van Zwieten, L.; Kammann, C.; Cayuela, M. L.; Singh, B. P.; Joseph, S.; Kimber, S.; Donne, S.; Clough, T.; Spokas, K. A., Biochar effects on nitrous oxide and methane emissions from soil. In *Biochar for Environmental Management: Science, Technology and Implementation*, Second edition. ed.; Lehmann, J.; Joseph, S., Eds. Routledge Taylor & Francis Group: London; New York, 2015; pp 489-420.
15. Lehmann, J.; Joseph, S., *Biochar for Environmental Management: Science, Technology and Implementation*. Second Edition ed.; Routledge: New York, NY, 2015.
16. Chun, Y.; Sheng, G.; Chiou, C. T.; Xing, B., Compositions and sorptive properties of crop residue-derived chars. *Environ. Sci. Technol.* **2004,** *38*, 4649-4655.
17. Yang, J.; Pignatello, J. J.; Yang, K.; Wu, W.; Lu, G.; Zhang, L.; Yang, C.; Dang, Z., Adsorption of Organic Compounds by Biomass Chars: Direct Role of Aromatic Condensation

(Ring Cluster Size) Revealed by Experimental and Theoretical Studies. *Environ. Sci. Technol.* **2021,** *55*, 1594-1603.

18. Tomków, K.; Jankowska, A.; Czechowski, F.; Siemieniewska, T., Activation of brown-coal chars with oxygen. *Fuel* **1977,** *56*, 101-106.

19. Tam, M. S.; Antal, M. J., Preparation of activated carbons from macadamia nut shell and coconut shell by air activation. *Ind. Eng. Chem. Res.* **1999,** *38*, 4268-4276.

20. Xiao, F.; Pignatello, J. J., Effects of Post-Pyrolysis Air Oxidation of Biomass Chars on Adsorption of Neutral and Ionizable Compounds. *Environ. Sci. Technol.* **2016,** *50*, 6276-6283.

21. Antal, M. J.; Grønli, M., The art, science, and technology of charcoal production. *Ind. Eng. Chem. Res.* **2003,** *42*, 1619-1640.

22. Li, J.; Li, Q.; Steinberg, C. E. W.; Zhao, Q.; Pan, B.; Pignatello, J. J.; Xing, B., Reaction of Substituted Phenols with Lignin Char: Dual Oxidative and Reductive Pathways Depending on Substituents and Conditions. *Environ. Sci. Technol.* **2020**.

23. Mia, S.; Dijkstra, F. A.; Singh, B., Aging Induced Changes in Biochar's Functionality and Adsorption Behavior for Phosphate and Ammonium. *Environ. Sci. Technol.* **2017,** *51*, 8359-8367.

24. Hale, S.; Hanley, K.; Lehmann, J.; Zimmerman, A.; Cornelissen, G., Effects of chemical, biological, and physical aging as well as soil addition on the sorption of pyrene to activated carbon and biochar. *Environ. Sci. Technol.* **2011,** *45*, 10445-10453.

25. Mukherjee, A.; Zimmerman, A.; Hamdan, R.; Cooper, W., Physicochemical changes in pyrogenic organic matter (biochar) after 15 months of field aging. *Solid Earth* **2014,** *5*, 693.

26. Nguyen, B. T.; Lehmann, J.; Hockaday, W. C.; Joseph, S.; Masiello, C. A., Temperature sensitivity of black carbon decomposition and oxidation. *Environ. Sci. Technol.* **2010,** *44*, 3324-3331.

27. Yang, Y.; Sheng, G., Pesticide adsorptivity of aged particulate matter arising from crop residue burns. *J. Agric. Food. Chem.* **2003,** *51*, 5047-5051.

28. Martin, S. M.; Kookana, R. S.; Van Zwieten, L.; Krull, E., Marked changes in herbicide sorption–desorption upon ageing of biochars in soil. *J. Hazard. Mater.* **2012,** *231*, 70-78.

29. Pignatello, J. J.; Uchimiya, M.; Abiven, S.; Schmidt, M. W., Evolution of biochar properties in soil. In *Biochar for Environmental Management*, Routledge: 2015; pp 227-266.

30. Xiao, F.; Gámiz, B.; Pignatello, J. J., Adsorption and desorption of nitrous oxide by raw and thermally air-oxidized chars. *Sci. Total Environ.* **2018,** *643*, 1436-1445.

31. Cao, X.; Xiao, F.; Duan, P.; Pignatello, J. J.; Mao, J.; Schmidt-Rohr, K., Effects of post-pyrolysis air oxidation on the chemical composition of biomass chars investigated by solid-state nuclear magnetic resonance spectroscopy. *Carbon* **2019,** *153*, 173-178.

32. Brewer, C. E.; Schmidt‐Rohr, K.; Satrio, J. A.; Brown, R. C., Characterization of biochar from fast pyrolysis and gasification systems. *Environmental Progress & Sustainable Energy: An Official Publication of the American Institute of Chemical Engineers* **2009,** *28*, 386-396.

33. Otake, Y.; Jenkins, R. G., Characterization of oxygen-containing surface complexes created on a microporous carbon by air and nitric acid treatment. *Carbon* **1993,** *31*, 109-121.

34. Goertzen, S. L.; Thériault, K. D.; Oickle, A. M.; Tarasuk, A. C.; Andreas, H. A., Standardization of the Boehm titration. Part I. CO2 expulsion and endpoint determination. *Carbon* **2010,** *48*, 1252-1261.

35. Sparks, D. L., *Methods of Soil Analysis. Part 3. Chemical Methods* American Society of Agronomy, Soil Science Society of America: 1996.

36. Luo, J.; Crittenden, J. C., Nanomaterial Adsorbent Design: From Bench Scale Tests to Engineering Design. *Environ. Sci. Technol.* **2019,** *53*, 10537-10538.

37. Bering, B. P.; Dubinin, M. M.; Serpinsky, V. V., Theory of volume filling for vapor adsorption. *Journal of Colloid and Interface Science* **1966,** *21*, 378-393.

38.Dubinin, M. M., Fundamentals of the theory of adsorption in micropores of carbon adsorbents: Characteristics of their adsorption properties and microporous structures. *Carbon* **1989,** *27*, 457-467.
39.Lattao, C.; Cao, X.; Mao, J.; Schmidt-Rohr, K.; Pignatello, J. J., Influence of Molecular Structure and Adsorbent Properties on Sorption of Organic Compounds to a Temperature Series of Wood Chars. *Environ. Sci. Technol.* **2014,** *48*, 4790-4798.
40.Bering, B. P.; Gordeeva, V. A.; Dubinin, M. M.; Efimova, L. I.; Serpinskii, V. V., Development of concepts of the volume filling of micropores in the adsorption of gases and vapors by microporous adsorbents. *Bulletin of the Academy of Sciences of the USSR, Division of chemical science* **1971,** *20*, 17-22.
41.Crittenden, J. C.; Sanongraj, S.; Bulloch, J. L.; Hand, D. W.; Rogers, T. N.; Speth, T. F.; Ulmer, M., Correlation of aqueous-phase adsorption isotherms. *Environmental Science & Technology* **1999,** *33*, 2926-2933.
42.Yang, K.; Xing, B., Adsorption of Organic Compounds by Carbon Nanomaterials in Aqueous Phase: Polanyi Theory and Its Application. *Chem. Rev.* **2010,** *110*, 5989-6008.
43.Kasozi, G. N.; Zimmerman, A. R.; Nkedi-Kizza, P.; Gao, B., Catechol and Humic Acid Sorption onto a Range of Laboratory-Produced Black Carbons (Biochars). *Environ. Sci. Technol.* **2010,** *44*, 6189-6195.
44.Chen, Z.; Xiao, X.; Chen, B.; Zhu, L., Quantification of chemical states, dissociation constants and contents of oxygen-containing groups on the surface of biochars produced at different temperatures. *Environ. Sci. Technol.* **2014,** *49*, 309-317.
45.Duan, P.; Schmidt-Rohr, K., Quick, selective NMR spectra of COH moieties in 13C-enriched solids. *J. Magn. Reson.* **2019,** *301*, 80-84.
46.Crank, J., *The mathematics of diffusion*. Oxford university press: 1979.
47.Franz, M.; Arafat, H. A.; Pinto, N. G., Effect of chemical surface heterogeneity on the adsorption mechanism of dissolved aromatics on activated carbon. *Carbon* **2000,** *38*, 1807-1819.
48.Li, L.; Quinlivan, P. A.; Knappe, D. R. U., Effects of activated carbon surface chemistry and pore structure on the adsorption of organic contaminants from aqueous solution. *Carbon* **2002,** *40*, 2085-2100.
49.Pendleton, P.; Wong, S. H.; Schumann, R.; Levay, G.; Denoyel, R.; Rouquero, J., Properties of activated carbon controlling 2-Methylisoborneol adsorption. *Carbon* **1997,** *35*, 1141-1149.
50.MacDonald, J. A. F.; Evans, M. J. B., Adsorption and enthalpy of phenol on BPL carbon. *Carbon* **2002,** *40*, 703-707.
51.Müller, E. A.; Rull, L. F.; Vega, L. F.; Gubbins, K. E., Adsorption of Water on Activated Carbons: A Molecular Simulation Study. *J. Phys. Chem.* **1996,** *100*, 1189-1196.
52.Müller, E. A.; Hung, F. R.; Gubbins, K. E., Adsorption of water vapor− methane mixtures on activated carbons. *Langmuir* **2000,** *16*, 5418-5424.
53.Schwarzenbach, R. P.; Gschwend, P. M.; Imboden, D. M., *Environmental organic chemistry*. John Wiley & Sons: 2016.
54.Molview. https://molview.org/?cid=15939 (March 20, 2021).
55.Kassab, E.; Castellà-Ventura, M.; Akacem, Y., Theoretical study of 4, 4′-bipyridine adsorption on the Brønsted acid sites of H-ZSM-5 zeolite. *The Journal of Physical Chemistry C* **2009,** *113*, 20388-20395.

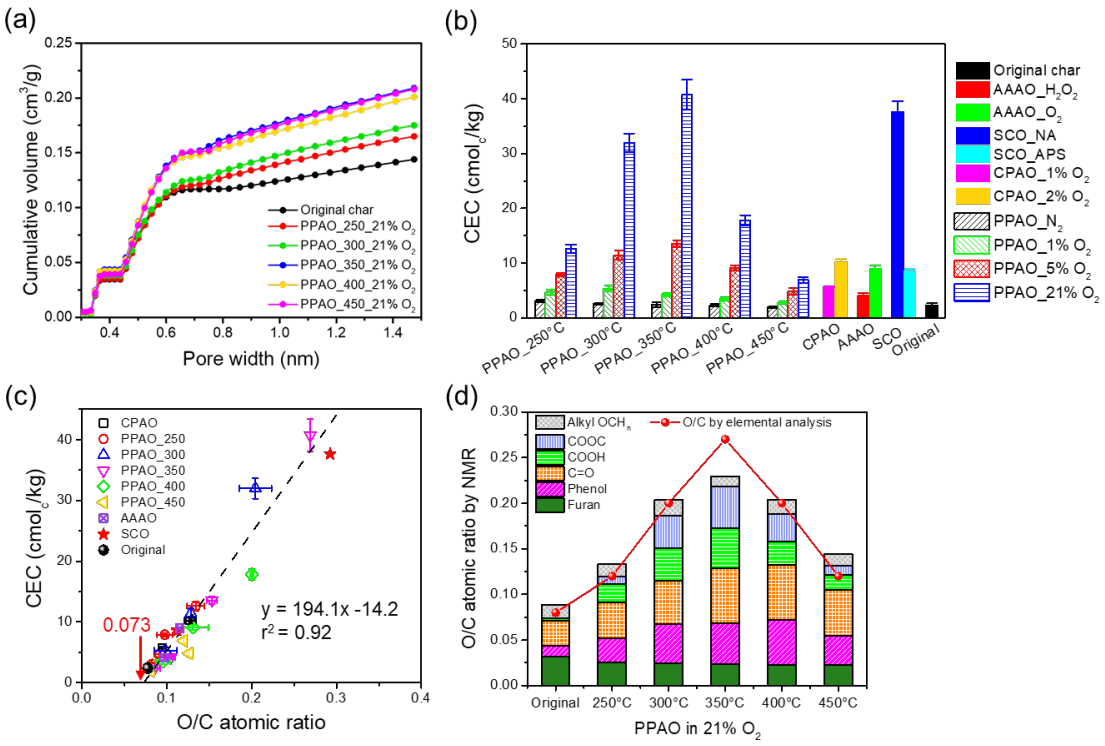

Figure 1. Select char characteristics: (a) cumulative micropore volume; (b) cation exchange capacity (CEC, pH 7.4); (c) CEC as a function of O/C ratio; (e) contribution to O/C ratio by different functional groups, calculated from NMR and titration data (red line represents O/C from elemental analysis). Other data are given in the SI.

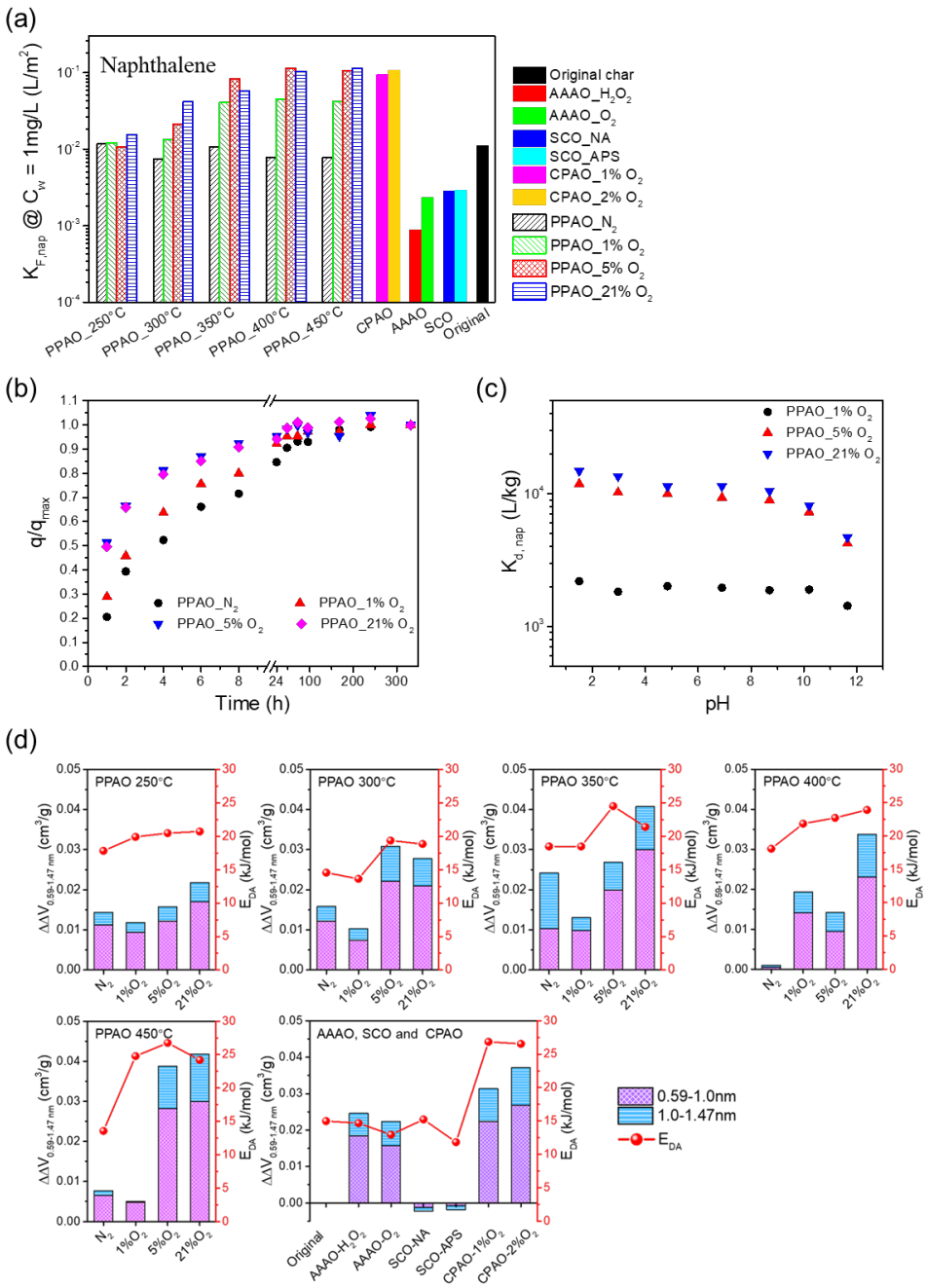

Figure 2. Collected data for naphthalene sorption: (a) $K_{F,nap}$ at unity concentration normalized by micropore surface area; (b) normalized rates of naphthalene uptake by chars treated by PPAO at 450 °C in different O_2 concentrations ([char] = 5 mg/60 ml; $[naphthalene]_0$ = 20 mg/L); (c) effect of pH on adsorption distribution ratio by chars treated by PPAO at 400 °C in different O_2 concentrations ([char] = 10 mg/60 ml; $[naphthalene]_0$ = 20 mg/L); (d) Dubinin-Ashtakhov characteristic sorption energy (E_{DA}, lines) compared with microporosity changes in the indicated region relative to the original char (bars).

674

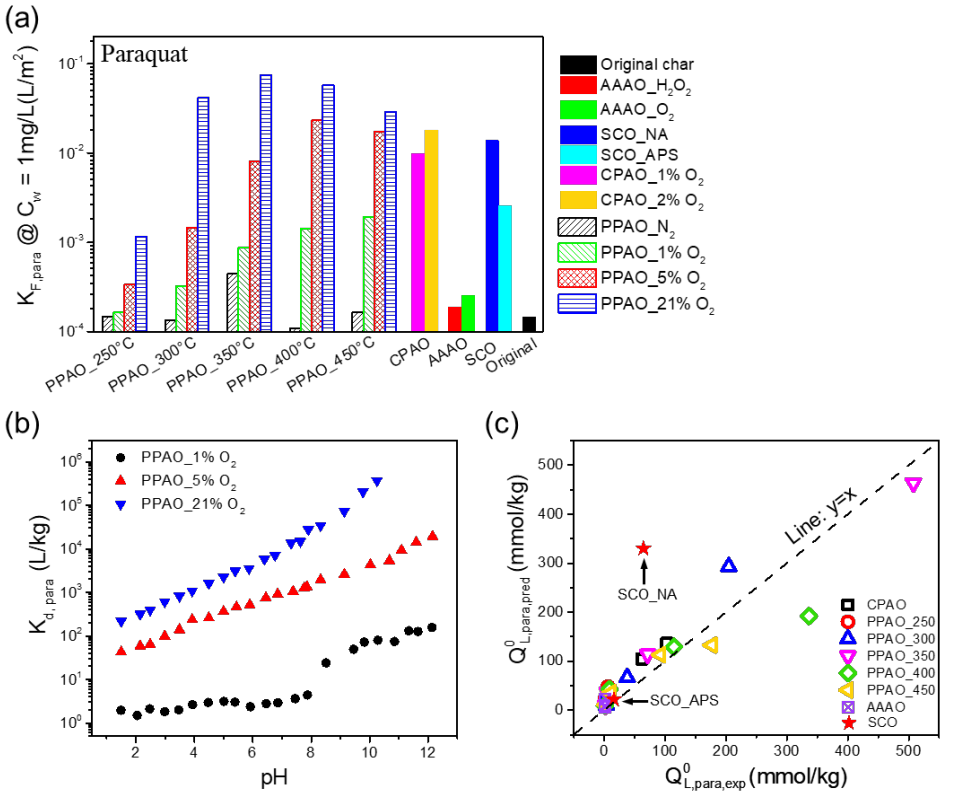

675

676

677 Figure 3. Collected data for paraquat sorption: (a) $K_{F,para}$ at unity concentration
678 normalized by micropore surface area; (b) effect of pH on distribution ratio by chars treated
679 by PPAO at 400 °C in different O_2 concentrations ([char] = 10 mg/15 ml; $[paraquat]_0$ =
680 28.6 mg/L); and (c) Experimental versus predicted values of $Q^0_{L,para}$ according to eq 14
681 (SCO values are excluded from the model of eq 14 but their predicted values are indicated
682 by the stars).